

RCWA-EIS method for interlayer grating coupling

CONGSHAN WAN,* THOMAS K. GAYLORD, AND MUHANNAD S. BAKIR

School of Electrical and Computer Engineering, Georgia Institute of Technology, Atlanta, Georgia 30332, USA

*Corresponding author: cwan3@gatech.edu

Received 22 April 2016; revised 8 June 2016; accepted 10 June 2016; posted 30 June 2016 (Doc. ID 263863); published 25 July 2016

The grating coupling efficiencies for interlayer connection (overlaid chips) were previously calculated using the new rigorous coupled-wave analysis equivalent-index-slab (RCWA-EIS) method. The chip-to-chip coupling efficiencies were determined for rectangular-groove (binary) gratings. In the present work, the search algorithms used in the RCWA-EIS method are optimized giving rise to improved definition of equivalent indices. Further, the versatility of the RCWA-EIS method is demonstrated by extending it to (nonbinary) parallelogramic gratings, sawtooth gratings, and volume gratings. The finite-difference time-domain method is used to verify the results. This demonstrates the flexibility of the RCWA-EIS method in analyzing arbitrary 1D gratings. © 2016 Optical Society of America

OCIS codes: (050.1950) Diffraction gratings; (050.1960) Diffraction theory; (060.1810) Buffers, couplers, routers, switches, and multiplexers; (130.0130) Integrated optics; (250.5300) Photonic integrated circuits.

<http://dx.doi.org/10.1364/AO.55.005900>

1. INTRODUCTION

There exist a great variety of grating structures that are being used in the field of optical interconnects (grating couplers [1–3]), optical components (polarizers [4], modulators [5], switches [6]), optoelectronics [7,8], sensors [9–11], antennas [12,13], etc. Surface-relief gratings, with a periodic variation in the surface profile, and volume holographic gratings, with a periodic variation in the refractive index of the material, comprise two categories of diffraction gratings. Surface-relief gratings have either a symmetric profile, e.g., binary gratings, triangular gratings, etc., or an asymmetric profile, e.g., parallelogramic gratings, sawtooth gratings, etc. It is well known that asymmetric profiles can enhance the grating diffraction efficiency into specific directions, and this property has been extensively applied in the design of optical components. Compared with volume gratings which are mostly polymer-based or glass-based, surface-relief gratings have reduced thicknesses, thus becoming a popular solution in compact interconnect technologies. In addition, surface-relief gratings can be fabricated using silicon-based materials, and they can be directly integrated into the CMOS platform. Volume gratings have been extensively explored in the field of data storage [14], optical correlation [15,16], optical information encryption [17], fiber communications [18], spectroscopy [19], etc., due to their large bandwidth storage capability and high sensitivity in wavelength and angle. The large variety and wide use of diffraction gratings make their design critically important.

Grating diffraction behaviors have been extensively studied and many theories have been proposed, including

coupled-wave approaches [20,21], modal approaches [22], perturbation methods [23,24], integral methods [25], differential methods [26], transmission line equivalent network approaches [24,27], amplitude transmittance approaches [28–30], coupled-mode approaches [31,32], and rigorous coupled-wave analysis (RCWA) methods [33,34]. The RCWA methods (also called Floquet modal methods) have been used to analyze accurately both surface-relief gratings and volume holographic gratings, and they are generally more computationally efficient than other methods. As a result, the RCWA methods have become popular choices in the design of grating structures. The most general goal of optimizing grating structures in various applications is to enhance the diffraction efficiency into specific orders. Previous optimization work on grating structures mainly used the finite-difference time-domain (FDTD) [35], COMSOL multiphysics [7], or CAMFR [36] simulation packages, which are typically very time-consuming. Genetic algorithms [37] or advanced search algorithms [38] have been used to optimize binary rectangular groove gratings, but the design parameters were limited and no information was provided regarding gratings with other profiles. The RCWA-leaky-wave (RCWA-LW) approach was proposed to optimize the grating out-diffraction behavior [39,40], but it requires careful choices of initial values for the Muller method to converge to reasonable results, thus making this method less practical. For surface-relief gratings used in sensors, optoelectronics, and optical components, no design optimizations have been provided, other than using the Floquet condition [4,7,9] or the surface plasmon resonance condition (for metallic biosensors) [9]. Therefore, a comprehensive design methodology that could

accurately simulate the diffraction behavior and efficiently optimize an arbitrary grating to achieve specific goals would be widely applicable.

In the present work, a general model based on the RCWA equivalent-index-slab (RCWA-EIS) method is introduced to analyze the diffraction behavior of arbitrary gratings in the chip-to-chip coupling configuration. This work is an extension of our previous work [41], in which a flexible and comprehensive tool for the interlayer optical coupling optimization of binary surface-relief gratings was introduced. Both works are based on the RCWA methods. The EIS method is introduced to find the radiation factor (α) of waveguide gratings, and it is especially useful in systems with large refractive index contrasts. The optimization tool based on the RCWA-EIS method is generally accurate, computationally efficient, and easy to implement. It accepts a large parameter space, e.g., coupling angle, grating period, grating height, etc., and requires no educated initial guesses on the parameters being optimized.

By representing the field amplitudes and phases at the boundaries and replacing the grating region with equivalent index slabs, the in-coupling/out-diffraction problem of any 1D grating structure can be simulated by the RCWA-EIS method. The in-plane transmitted power can also be calculated by subtracting the out-diffraction power from the total incident power. The purpose of this paper is to verify further the RCWA-EIS method by applying it to nonbinary grating structures, such as parallelogramic gratings, sawtooth gratings, and volume gratings. Furthermore, the search algorithms used in our previous work are optimized and these new algorithms are found to be more stable and computationally efficient than the original algorithms.

2. GRATING SIMULATION MODELS

The interlayer grating coupling problem is schematically depicted in Fig. 1. Two types of surface-relief gratings, namely parallelogramic gratings and sawtooth gratings, as well as volume gratings with sinusoidally varying refractive indices are considered here. Some basic parameters involved in the models are as follows: free-space wavelength of incident light λ_0 , coupling angle in the cover θ , grating thickness t_g , waveguide thickness t_w , grating fill factor f , grating period Λ , number of grating period N , and grating slant angle φ (for parallelogramic and volume gratings). TE (y) polarized planar incidence is considered in all the models. The formulations of the grating models follow the previous RCWA work [33,34,41,42]. The

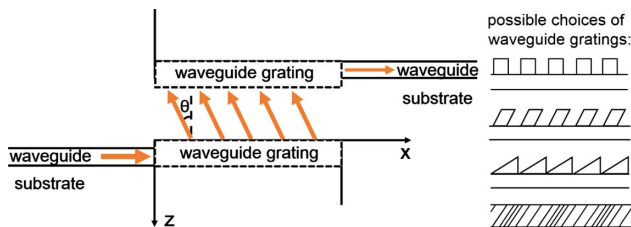


Fig. 1. Schematic representation (not to scale) of the grating-to-grating coupling process. The waveguide grating region indicated by the dashed box represents one of the grating structures at the right side of the figure.

permittivity formulations of each type of grating are introduced in Appendix A.

3. SEARCH ALGORITHMS

In the RCWA-EIS method, the grating layer is replaced by multiple homogenous slabs with specified refractive indices. A total of four equations related to the E fields and H fields of each of the 0 order and +1 order are involved (Equations (28)–(31) in our previous work [41]). The MATLAB function *fsolve* with the Levenberg–Marquardt (LM) algorithm was used to find the equivalent indices such that the function values of the four equations are close to zero. The LM algorithm minimizes the sum of squares of the functions, and the nonlinear system it deals with could be underdetermined, critical-sized, or overdetermined; that is, the number of unknowns could be greater than, equal to, or less than the number of equations. In our previous paper, the number of equivalent slabs, L_{eq} , was set to be no less than 4. For some cases, $L_{eq} = 4$ did not produce small function values, e.g., function values > preset function tolerance. In these cases, the method increased L_{eq} and *fsolve* was run again, which inevitably increases the calculation time. After the equivalent indices were determined, *fsolve* was used once again to find the radiation factor α in the multilayer structure. This step involves the two equations relating the reflected amplitude and the transmitted amplitude for each diffracted order (the equations below Eq. (33) in [41]) that are solved for the one unknown α . The resulting least-squares problem was solved using *fsolve* with the LM algorithm. However, the lower and upper bound of α cannot be defined in *fsolve* and this may lead to non-physically small or negative values of α .

In the present work, we introduce the use of the trust-region-dogleg (TRD) algorithm of *fsolve* to find the equivalent indices. This algorithm is specially designed to solve nonlinear equations, and it requires the number of equations be the same as the number of unknowns (here, $L_{eq} = 4$). The TRD algorithm usually gives small function values, e.g., less than 1×10^{-8} . The resulting four equivalent indices are verified further by calculating the propagation constant in the multilayer structure consisting of the cover, the four equivalent index slabs, the original waveguide, and the substrate, using the formulation reported in [43]. The calculated propagation constant β_{eq} is then compared with $k_{x,+1}$ (the propagation constant of the coupled order along the x direction). The radiation factor α , as the variable in the optimization, is found by finding the value that minimizes the sum of the norms of the two equations relating the reflected and transmitted amplitudes. This step is achieved by using the MATLAB function *fsolve* with the LM algorithm.

Attempts to restrict the search range for α based on prior knowledge of grating diffraction behavior (e.g., $0 < \alpha < 0.01$ for volume grating) were not successful when the global minimum of the function was outside of that range. If α is restricted to be in a range where the function is monotonic, the resulting optimized variable value will lie on the boundary of the range. Therefore, no range is imposed on the search of α . This freedom, however, may occasionally result in an unreasonable value of α , e.g., negative, extremely small ($< 10^{-4}$), or extremely large (> 0.1). These numerical artifacts are due to the finite precision

used in the computation. In many cases, these nonphysical values of α may be avoided by slightly changing the values ($\pm 10^{-4}$) of input parameters, e.g., coupling angle, grating period, grating height, etc.

4. RESULTS AND DISCUSSION

A. Grating Diffraction Efficiencies

For the analysis of surface-relief gratings, three grating parameters, namely coupling angle (θ), grating period (Λ), and grating thickness (t_g), are variables to be optimized. The known parameters are as follows: free-space wavelength $\lambda_0 = 1.55 \mu\text{m}$, cover refractive index $n_c = 1$ (air), substrate refractive index $n_s = 1.45$ (SiO_2), grating groove refractive index $n_{gr} = 1$ (air), grating ridge refractive index $n_{rd} = 2.46$ (Si_3N_4), waveguide refractive index $n_w = 3.45$ (Si), grating fill factor $f = 0.5$ (for binary and parallelogramic gratings), and waveguide thickness $t_w = 0.22 \mu\text{m}$. The fundamental mode propagation constant of the $0.22 \mu\text{m}$ -thick waveguide is calculated to be $\beta_0 = 11.3710 \mu\text{m}^{-1}$. The total number of space harmonics is set to be $n = 7$.

For the analysis of volume gratings, three grating parameters, namely coupling angle (θ), grating period (Λ), and slant angle (φ), are variables to be optimized. The known parameters are as follows: free-space wavelength $\lambda_0 = 1.55 \mu\text{m}$, cover refractive index $n_c = 1$ (air), substrate refractive index $n_s = 1.45$ (SiO_2), waveguide refractive index $n_w = 1.8$ (generic material not specified), average grating refractive index $n_g = 1.8$ (chosen for the FDTD calculation), grating refractive index modulation $\Delta n_g = 0.1$ ($\Delta \epsilon \approx 2n_g \Delta n_g$), waveguide thickness $t_w = 0.4 \mu\text{m}$, and grating thickness $t_g = 0.4 \mu\text{m}$. The fundamental mode propagation constant of the $0.4 \mu\text{m}$ -thick waveguide is calculated to be $\beta_0 = 6.3008 \mu\text{m}^{-1}$. The total number of space harmonics is again set to be $n = 7$.

The optimization of the grating parameters is carried out using the MATLAB function *fmincon*. The grating is designed to couple the $i = +1$ order diffracted light into/out of the waveguide, and thus the target of optimization is the diffraction efficiency of the $i = +1$ order ($DE_{c,+1}$), and $k_{x,+1}$ should be comparable to β_0 . Optimizing the single-grating diffraction efficiency $DE_{c,+1}$ is the same as optimizing the grating-to-grating coupling efficiency, which is approximated by $DE_{c,+1}^2$. To ensure the maximum diffraction efficiency of the $i = +1$ order, diffraction orders other than $i = 0$ and $i = +1$ should not propagate. Furthermore, to ensure the correctness of the four equivalent indices, the propagation constant calculated using the equivalent indices, β_{eq} (taking the real part), should be comparable to $k_{x,+1}$, and the difference between these two values is restricted to be less than 2%. As a result, the nonlinear constraints in the *fmincon* function is thus set as follows: (1) $|\beta_0 - k_{x,+1}| < k_0 n_w - \beta_0$, (2) $k_{x,-1} > k_0 n_w$, (3) $|k_{x,+1} - \beta_{\text{eq}}|/|k_{x,+1}| < 0.02$, and (4) $\alpha > 0$. The lower and upper bounds of the three variables $[\theta, \Lambda, t_g]$ are set to be $[0.1 \text{ rad } (5.73^\circ), 0.3 \mu\text{m}, 0.05 \mu\text{m}]$ and $[\pi/4 \text{ rad } (45^\circ), 1.55 \mu\text{m}, 0.4 \mu\text{m}]$, respectively. Taking into account fabrication limits, the thickness of the Si_3N_4 layer should be less than $0.4 \mu\text{m}$ [37], and the minimum coupling angle should be set to $0.1 \text{ rad } (5.73^\circ)$ to reduce the possibility of coupling into -1 diffraction order. For the volume grating, the lower and upper bounds of $[\theta, \Lambda, \varphi]$ are set to be

$[0.1 \text{ rad } (5.73^\circ), 0.2 \mu\text{m}, 0.3 \text{ rad } (17.19^\circ)]$ and $[0.4 \text{ rad } (22.91^\circ), 1 \mu\text{m}, 1.3 \text{ rad } (74.48^\circ)]$, respectively.

For all the grating structures presented in this paper, the MATLAB function *fsolve* with the TRD algorithm is used to find the equivalent indices. The function tolerance of *fsolve* is set to be 1×10^{-8} . The MATLAB function *fsolve* with the LM algorithm is used to find the radiation factor of the multilayer structure, and its function tolerance is set to be 1×10^{-8} . The optimization is carried out using the MATLAB function *fmincon* with nonlinear constraints specified above. Parameter sweep of initial values, e.g., $[\theta, \Lambda, t_g]$ for the surface-relief gratings and $[\theta, \Lambda, \varphi]$ for the volume gratings, can be conducted to avoid finding of unreasonable α . Normally, α for parallelogramic gratings, sawtooth gratings, and volume gratings are in the range of $[0.01, 0.1]$, $[0.001, 0.02]$, and $[0.001, 0.02]$, respectively. In general, the search algorithms work well for grating structures with relatively large α , e.g., parallelogramic gratings and binary gratings; for grating structures with relatively small α , e.g., sawtooth gratings and volume gratings, parameter sweep of initial values is highly recommended.

B. Parallelogramic Grating Coupler

According to Li and Sheard [44], the optimized slant angle for a forward-slanted parallelogramic grating (geometry defined in Appendix A) is defined as

$$\varphi = \arcsin \left(\lambda_0 / \left(\Lambda \sqrt{n_{gr}^2 + f(n_{rd}^2 - n_{gr}^2)} - \beta_0^2 + 2\beta_0 \lambda_0 / \Lambda \right) \right). \quad (1)$$

Therefore, the slant angle φ is determined once the grating period Λ is found for a given material system.

Six optimized parallelogramic gratings, four forward-slanted cases (case f-pa-1 to case f-pa-4) and two backward-slanted cases (case b-pa-1 and case b-pa-2), are summarized in Table 1 which includes the optimized parameters θ , Λ , and φ as well as the resulting parameters, such as the preferential coupling ratio in the $+1$ order ($PC_{c,+1}$), single-grating diffraction efficiency of $+1$ order at $N = 50$ ($DE_{c,+1}$), coupled mode propagation constant ($\beta = k_{x,+1}$), and the radiation factor (α). The single-grating diffraction efficiencies ($DE_{c,+1}$) as a function of number of grating periods (N) for the parallelogramic gratings are shown in Fig. 2. The results obtained from the RCWA-EIS method demonstrate good agreement with those calculated by the FDTD calculations. Some of the data plots corresponding to the FDTD calculations exhibit irregularity due to the numerical instability induced by the slanted grating structure. The error may be reduced by increasing the resolution of the FDTD simulation, but it requires more computation time. It is observed that the optimized forward-slanted gratings have much larger diffraction efficiencies ($DE_{c,+1} > 60\%$ at $N = 50$) than the optimized backward-slanted gratings ($DE_{c,+1} \approx 40\%$ at $N = 50$), which agrees with the conclusion that forward-slanted parallelogramic gratings give higher diffraction efficiencies as stated in Li and Sheard [44]. It is also observed that the preferential coupling ratios ($PC_{c,+1}$) of the forward-slanted parallelogramic gratings are much greater than 0.5, which is a good demonstration of the benefit of using asymmetric grating profiles. It is known that gratings with symmetric profiles, e.g., sinusoidal and

Table 1. Optimized Parameters and Calculated Single-Grating Diffraction Efficiencies for Parallelogramic Gratings^a

| Case Number | Initial Values | | | Optimized Values | | | | | | | |
|-------------|----------------------|-----------------------------|-------------------------|----------------------|-----------------------------|-------------------------|-----------------------|-------------|-------------------------|--------------------------------|---------------------------------|
| | θ [rad (deg)] | Λ [μm] | t_g [μm] | θ [rad (deg)] | Λ [μm] | t_g [μm] | φ [rad (deg)] | $PC_{c,+1}$ | $DE_{c,+1}$ at $N = 50$ | β [μm^{-1}] | α [μm^{-1}] |
| f-pa-1 | 0.30 (17.19°) | 0.55 | 0.30 | 0.3005 (17.22°) | 0.5373 | 0.3124 | 0.9942 (54.96°) | 0.8175 | 0.6354 | 10.4950 | 0.0279 |
| f-pa-2 | 0.25 (14.32°) | 0.70 | 0.30 | 0.1935 (11.09°) | 0.5706 | 0.2994 | 0.9665 (55.38°) | 0.7330 | 0.6025 | 10.2310 | 0.0302 |
| f-pa-3 | 0.25 (14.32°) | 0.55 | 0.30 | 0.2916 (16.71°) | 0.5573 | 0.3323 | 0.9770 (55.98°) | 0.7600 | 0.6622 | 10.1087 | 0.0368 |
| f-pa-4 | 0.10 (5.73°) | 0.52 | 0.39 | 0.1956 (11.21°) | 0.5589 | 0.3087 | 0.9757 (55.90°) | 0.7923 | 0.5828 | 10.4542 | 0.0238 |
| b-pa-1 | 0.10 (5.73°) | 0.53 | 0.34 | 0.2242 (12.85°) | 0.5407 | 0.3095 | 0.9911 (56.79°) | 0.8038 | 0.4246 | 10.7192 | 0.0139 |
| b-pa-2 | 0.11 (6.30°) | 0.48 | 0.12 | 0.1507 (8.63°) | 0.4912 | 0.1575 | 1.0418 (59.69°) | 0.8006 | 0.3609 | 12.1829 | 0.0122 |

^aForward-slanted parallelogramic gratings are indicated by “f-pa,” and backward-slanted ones are indicated by “b-pa.”

rectangular, radiate the incident power (or guided power) almost equally into the cover and the substrate, resulting in a preferential coupling ratio (or radiation directionality) close

to 50% provided the refractive index of the cover is comparable to that of the substrate. On the contrary, gratings with asymmetric profiles, e.g., blazed (trapezoidal, sawtooth, or triangular) and parallelogramic, emit more than 90% of the radiated power into the cover [45–48]. Nevertheless, the radiation factor α , defined as the radiated power per unit grating length, of the blazed grating is very small, and thus a longer grating is required to radiate the same amount of incident (or guided) power. Researchers have already found that a parallelogramic grating provides both a larger radiation factor and higher radiation directionality than gratings with other tooth profiles [44,49]. Therefore, parallelogramic gratings offer the benefits of simultaneously obtaining high diffraction efficiency and high device compactness. From Tables 1–3, it is found that the radiation factors α of the forward-slanted parallelogramic gratings are relatively large compared to those of other grating profiles discussed in this paper. In spite of their relatively complex profiles, parallelogramic gratings can be fabricated using the methods such as those presented in [49,50].

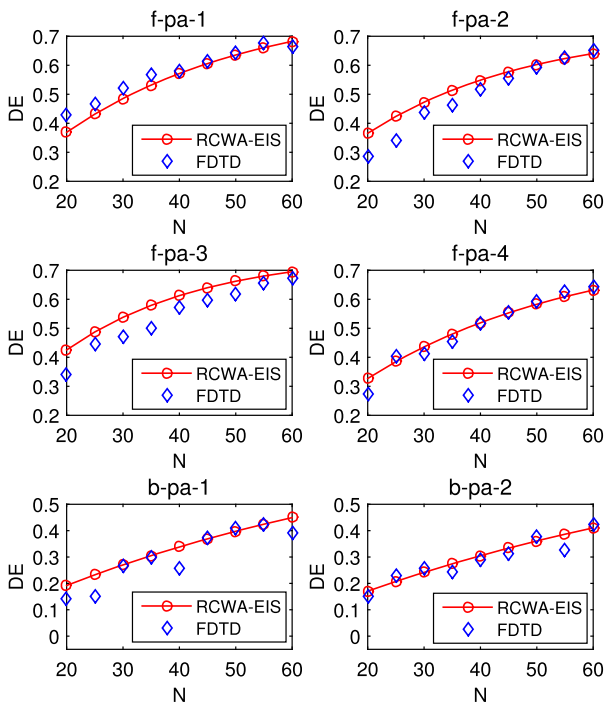


Fig. 2. Single-grating diffraction efficiency ($DE_{c,+1}$) as a function of number of periods (N) or grating length ($\ell = N\Lambda$) for parallelogramic gratings, where Λ is given in Table 1.

C. Sawtooth Grating Coupler

Six optimized sawtooth gratings, four forward-slanted cases (case f-saw-1 to case f-saw-4) and two backward-slanted cases (case b-saw-1 and case b-saw-2), are summarized in Table 2. The single-grating diffraction efficiencies ($DE_{c,+1}$) as a function of number of grating periods (N) for the sawtooth gratings are shown in Fig. 3. The results obtained from the RCWA-EIS method demonstrate good agreement with those from FDTD calculations. The optimized forward-slanted gratings have larger diffraction efficiencies ($DE_{c,+1} \approx 30\%$ at $N = 50$) than the optimized backward-slanted gratings ($DE_{c,+1} \approx 20\%$ at $N = 50$), though the improvement of the forward-slanted profile is not as

Table 2. Optimized Parameters and Calculated Single-Grating Diffraction Efficiencies for Sawtooth Gratings^a

| Case Number | Initial Values | | | Optimized Values | | | | | | | |
|-------------|----------------------|-----------------------------|-------------------------|----------------------|-----------------------------|-------------------------|-------------|-------------------------|--------------------------------|---------------------------------|--|
| | θ [rad (deg)] | Λ [μm] | t_g [μm] | θ [rad (deg)] | Λ [μm] | t_g [μm] | $PC_{c,+1}$ | $DE_{c,+1}$ at $N = 50$ | β [μm^{-1}] | α [μm^{-1}] | |
| f-saw-1 | 0.10 (5.73°) | 0.47 | 0.37 | 0.2345 (13.44°) | 0.4793 | 0.3667 | 0.7931 | 0.2929 | 12.1672 | 0.0096 | |
| f-saw-2 | 0.11 (6.30°) | 0.53 | 0.36 | 0.1201 (6.88°) | 0.5406 | 0.3712 | 0.7889 | 0.3085 | 11.1369 | 0.0092 | |
| f-saw-3 | 0.10 (5.73°) | 0.52 | 0.31 | 0.2057 (11.79°) | 0.5434 | 0.2872 | 0.8033 | 0.3370 | 10.7348 | 0.0010 | |
| f-saw-4 | 0.13 (7.45°) | 0.58 | 0.25 | 0.1710 (9.80°) | 0.4866 | 0.3572 | 0.7922 | 0.2790 | 12.2226 | 0.0089 | |
| b-saw-1 | 0.10 (5.73°) | 0.60 | 0.10 | 0.2317 (13.28°) | 0.5356 | 0.2079 | 0.5840 | 0.2366 | 10.7997 | 0.0097 | |
| b-saw-2 | 0.25 (14.32°) | 0.50 | 0.25 | 0.2376 (13.61°) | 0.5088 | 0.2409 | 0.4864 | 0.1940 | 11.3951 | 0.0099 | |

^aForward-slanted sawtooth gratings are indicated by “f-saw,” and backward-slanted ones are indicated by “b-saw.”

Table 3. Optimized Parameters and Calculated Single-Grating Diffraction Efficiencies for Volume Gratings with Sinusoidally Varying Indices

| Case Number | Initial Values | | | Optimized Values | | | | | | |
|-------------|-------------------------|--------------------------------|--------------------------|-------------------------|--------------------------------|--------------------------|-------------|----------------------------|-----------------------------------|------------------------------------|
| | θ [rad (deg)] | Λ [μm] | φ [rad (deg)] | θ [rad (deg)] | Λ [μm] | φ [rad (deg)] | $PC_{c,+1}$ | $DE_{c,+1}$ at $N = 50$ | β [μm^{-1}] | α [μm^{-1}] |
| vol-1 | 0.30 (17.19°) | 0.70 | 1.20 (68.75°) | 0.1041 (5.96°) | 0.7019 | 0.9255 (53.03°) | 0.5968 | 0.3010 | 6.7298 | 0.0098 |
| vol-2 | 0.20 (11.46°) | 0.80 | 1.10 (63.03°) | 0.2107 (12.07°) | 0.7864 | 1.1041 (63.26°) | 0.6022 | 0.2810 | 6.2883 | 0.0080 |
| vol-3 | 0.30 (17.19°) | 0.70 | 1.10 (63.03°) | 0.2933 (16.80°) | 0.6974 | 0.9630 (55.18°) | 0.6274 | 0.2684 | 6.2235 | 0.0079 |
| vol-4 | 0.20 (11.46°) | 0.80 | 1.00 (57.30°) | 0.1847 (10.58°) | 0.8318 | 1.0985 (62.94°) | 0.7415 | 0.2722 | 5.9822 | 0.0055 |

significant as in the cases of parallelogramic gratings. The preferential coupling ratios of the forward-slanted sawtooth gratings are also much larger than 50%. Aoyagi *et al.* [51] reported that the blazed grating can direct 97% of the total radiated power into the desired angle. Although the preferential coupling ratios of sawtooth gratings shown in Table 2 are approximately 80%, they can be optimized if the target function is $PC_{c,+1}$ rather than $DE_{c,+1}$. Nevertheless, the resulting diffraction efficiencies are small due to the small radiation factor common in blazed gratings.

D. Volume Grating Coupler

The volume grating is taken to be a section of the waveguide with sinusoidal index modulation; that is, the volume grating is in the waveguide instead of on top of the waveguide as in the previous examples. Four optimized volume gratings are summarized in Table 3. The single-grating diffraction efficiencies ($DE_{c,+1}$) as a function of number of grating periods (N) for the volume gratings are shown in Fig. 4. The results obtained from the RCWA-EIS method demonstrate good agreement with those calculated by the FDTD calculations. As the grating is a part

of the waveguide, the guided field is largely affected by the index-varying region. Nevertheless, the diffraction efficiency is relatively small due to the small δn_g used in this model. Since the majority of the volume gratings are made of polymer with typical indices from 1.3 to 1.7, and the index modulation Δn_g is usually less than 0.1, the diffraction efficiency of the volume gratings should not be compared with those of surface-relief gratings with large index differences. Here, the results are used to demonstrate the feasibility of the RCWA-EIS method in simulating arbitrary volume gratings.

E. Search Algorithms

The search algorithms proposed in this work and our previous work are compared in this section. The present algorithm, using *fsolve* with TRD and *fsolve* with LM to find $n_{g,\text{eq}}$ and α , respectively, will be designated as Method 1, while the previous algorithm, using *fsolve* with LM and *fsolve* with LM to find $n_{g,\text{eq}}$ and α , respectively, will be designated as Method 2. Binary gratings are used to test and compare the two methods. The material system of the binary gratings are exactly the same as those of the surface-relief gratings discussed above. Two representative cases are summarized in Table 4. Three grating parameters [θ , Λ , t_g] are [0.3001 rad (17.19°), 0.6000 μm , 0.2340 μm], and [0.2801 rad (16.05°), 0.5311 μm , 0.2432 μm] for Case 1 and Case 2, respectively. The results obtained from Method 1 are verified by FDTD simulations,

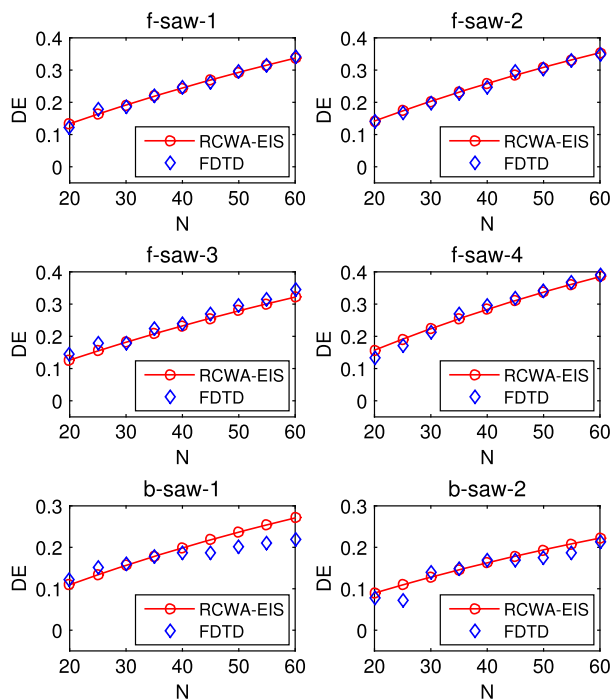


Fig. 3. Single-grating diffraction efficiency ($DE_{c,+1}$) as a function of number of periods (N) or grating length ($\ell = N\Lambda$) for sawtooth gratings, where Λ is given in Table 2.

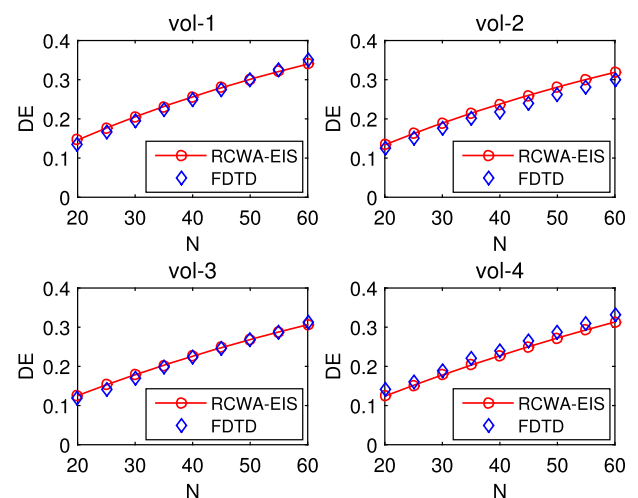


Fig. 4. Single-grating diffraction efficiency ($DE_{c,+1}$) as a function of number of periods (N) or grating length ($\ell = N\Lambda$) for volume gratings, where Λ is given in Table 3.

Table 4. Comparison of Two Search Algorithms for the Two Binary Cases

| Quantity | Binary Case 1 | | | | Binary Case 2 | | | |
|---------------------------------|----------------------|----------------------|-----------------------|------------------------|------------------------|------------------------|----------------------|-------------|
| | Method 1 | | Method 2 | | Method 1 | | Method 2 | |
| | Iteration 1 | Iteration 2 | Iteration 1 | Iteration 1 | Iteration 1 | Iteration 2 | Iteration 3 | Iteration 4 |
| $n_{g,eq1}$ | 0.9876 - 4.8328j | -0.9890 + 4.7668j | 3.2720 - 5.1527j | 3.1778 - 4.6698j | 3.3593 - 4.7174j | 3.1524 - 3.9359j | 4.1782 - 8.1183j | |
| $n_{g,eq2}$ | 6.4085 + 1.5522j | 6.3905 + 1.5414j | 6.8213 + 2.0172j | 6.7104 + 2.0089j | 6.9422 + 2.1722j | 6.4213 + 2.0822j | 7.2202 + 1.6512j | |
| $n_{g,eq3}$ | 5.0465 - 3.7908j | 5.0146 - 3.8093j | 6.6727 - 4.1771j | 6.5670 - 4.2384j | 4.4964 - 3.3923j | 3.1862 - 0.5344j | 5.1783 + 1.3997j | |
| $n_{g,eq4}$ | 2.8623 + 1.2968j | 2.9104 + 1.3127j | 3.1786 + 1.6805j | -3.4811 - 1.8417j | 5.2289 - 2.5631j | 5.6797 - 3.2270j | 4.0158 - 2.0805j | |
| $n_{g,eq5}$ | - | - | - | - | -3.6444 - 2.7911j | 2.7077 - 0.8281j | 6.9473 - 2.9823j | |
| $n_{g,eq6}$ | - | - | - | - | - | -3.6547 - 2.6036j | 1.1492 - 0.5535j | |
| $n_{g,eq7}$ | - | - | - | - | - | 5.8 × 10 ⁻² | -3.2478 - 2.2459j | |
| func. val. | 1 × 10 ⁻⁹ | 1 × 10 ⁻⁴ | 1 × 10 ⁻¹³ | 2.4 × 10 ⁻³ | 1.6 × 10 ⁻² | - | 4 × 10 ⁻⁴ | |
| α (μm^{-1}) | 0.0375 | 0.0352 | 0.0445 | 0.0428 | 1.6284 | 0.617 | 0.0101 | |
| $PC_{c,+1}$ | 0.4914 | 0.4913 | 0.5011 | - | - | - | 0.5010 | |

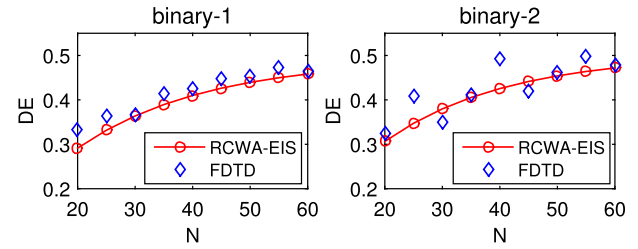


Fig. 5. Single-grating diffraction efficiency ($DE_{c,+1}$) as a function of number of periods (N) or grating length ($l = N\Lambda$) for binary gratings, where Λ is given in Section 4.E.

as shown in Fig. 5. Method 1 only requires one calculation to determine the four equivalent indices, while Method 2 may require more iterations (adding one layer per iteration) in order to achieve function tolerance, which is set to be 1×10^{-3} in this analysis. From Table 4, it is observed that the function values resulting from Method 1 are extremely small (1×10^{-9} and 1×10^{-13} for the two cases), which means the four equivalent indices are well chosen. Case 1 gives an example in which Method 2 requires only one iteration, and the resulting α is comparable to that obtained from Method 1. In Case 2, Method 2 requires four iterations in order to achieve the function tolerance, but the final result is not correct. Case 2 is a representation in which Method 2 fails to find a reasonable α but Method 1 succeeds. The validity of Method 2 greatly depends on the function tolerance. If the function tolerance is set to be 1×10^{-2} , Method 2 would iterate one time to give a reasonable $\alpha = 0.0428$ for Case 2, as indicated in Table 4. As a result, Method 1 is a more robust approach in determining the radiation factor. The equivalent indices result from satisfying all of the field amplitude and phase conditions at the boundaries. The physical interpretation of their values is not obvious.

5. CONCLUSIONS

The present work validates the RCWA-EIS method by applying it to parallelogramic gratings, sawtooth gratings, and volume gratings. In general, the RCWA-EIS method can be applied to any 1D grating structure. The improved search algorithms presented result in a better set of equivalent indices. The RCWA-EIS method is generally robust for grating structures with large radiation factors ($\alpha > 0.01 \mu\text{m}^{-1}$), though it may require multiple trials with different initial guesses α_0 for grating structures with small radiation factors ($\alpha < 0.01 \mu\text{m}^{-1}$). As a simplified version of the RCWA-LW approach, the RCWA-EIS method takes into account two propagating diffraction orders but neglects higher-order diffracted waves that are evanescent. The RCWA-EIS method is currently being applied to modeling the effect of rotational misalignment errors in grating-to-grating couplers for the cases where the 0 and +1 diffracted orders are dominant.

APPENDIX A

A. Parallelogramic Grating

For an arbitrary surface-relief grating, the relative permittivity of the grating region can be expressed as the Fourier series along the x direction:

$$\varepsilon_g(x) = \varepsilon_{gr} + (\varepsilon_{rd} - \varepsilon_{gr}) \sum_b \tilde{\varepsilon}_b \exp(jbKx), \quad (\text{A1})$$

where $\tilde{\varepsilon}_b$ is the b -th Fourier coefficient, K is the grating vector magnitude ($K = \frac{2\pi}{\Lambda}$), and ε_{gr} and ε_{rd} are the permittivity of the grating groove and grating ridge, respectively. A nonbinary grating can be horizontally sliced into a total of L sublayers, and each sublayer can be represented by a binary grating. For each sublayer, the matrix of permittivity coefficient $\tilde{\varepsilon}_b$ as defined in Eq. (17) in our previous paper [41] is no longer symmetric.

Figure 6 shows two possible parallelogramic gratings, one with slant angle $\varphi < 90^\circ$ (designated as “forward-slanted” in this paper) and the other with $\varphi > 90^\circ$ (designated as “backward-slanted”). The guided wave is incident on the grating in the $+x$ direction from the left. If $\Delta < W$, where $\Delta = t_g / \tan \varphi$ and $W = (1 - f)\Lambda$ as shown in Fig. 7, the b -th Fourier coefficient of the l -th sublayer of the forward-slanted parallelogramic grating can be expressed as

$$\tilde{\varepsilon}_{l,b}(x) = \frac{1}{\Lambda} \int_{\Delta - l\delta}^{\Delta - l\delta + f\Lambda} \exp(-jbKx) dx, \quad (\text{A2})$$

where $\delta = \Delta/L$. If $\Delta > W$, the parallelogramic grating will be separated into two sections, and the top and the bottom sections are divided into L_1 and L_2 slices, respectively. The b -th Fourier coefficient of the l -th sublayer of the forward-slanted parallelogramic grating is expressed as

$$\tilde{\varepsilon}_{l,b}(x) = \begin{cases} \frac{1}{\Lambda} \left[\int_0^{\rho - l\delta_1} \exp(-jbKx) dx + \int_{\rho - l\delta_1 + W}^{\Lambda} \exp(-jbKx) dx \right], & l \in [1, L_1] \\ \frac{1}{\Lambda} \int_{W - l\delta_2}^{\Lambda - l\delta_2} \exp(-jbKx) dx, & l \in [L_1 + 1, L_1 + L_2] \end{cases}, \quad (\text{A3})$$

where $\rho = \Delta - W$, $t_2 = W \tan \varphi$, $t_1 = t_g - t_2$, $\delta_1 = t_1 / (L_1 \tan \varphi)$, and $\delta_2 = t_2 / (L_2 \tan \varphi)$, and t_1 and t_2 are the thickness of the top and bottom layers, respectively.

Similarly, the $\tilde{\varepsilon}_{l,b}(x)$ of the l -th sublayer of the backward-slanted parallelogramic grating can be expressed as

$$\tilde{\varepsilon}_{l,b}(x) = \frac{1}{\Lambda} \int_{W - \Delta + (l-1)\delta}^{\Lambda - \Delta + (l-1)\delta} \exp(-jbKx) dx \quad (\text{A4})$$

for $\Delta < W$, and

$$\tilde{\varepsilon}_{l,b}(x) = \begin{cases} \frac{1}{\Lambda} \left[\int_0^{\Lambda - \Delta + (l-1)\delta_1} \exp(-jbKx) dx + \int_{\Lambda - \rho + (l-1)\delta_1}^{\Lambda} \exp(-jbKx) dx \right], & l \in [1, L_1] \\ \frac{1}{\Lambda} \int_{(l-1)\delta_2}^{(l-1)\delta_2 + f\Lambda} \exp(-jbKx) dx, & l \in [L_1 + 1, L_1 + L_2] \end{cases} \quad (\text{A5})$$

for $\Delta > W$.

B. Sawtooth Grating

Figure 8 shows two kinds of sawtooth gratings, namely (a) “forward-slanted” and (b) “backward-slanted.” The b -th Fourier coefficient of the l -th sublayer is expressed as

$$\tilde{\varepsilon}_{l,b}(x) = \frac{1}{\Lambda} \int_{\Lambda - l\delta}^{\Lambda} \exp(-jbKx) dx \quad (\text{A6})$$

for the forward-slanted sawtooth grating, and

$$\tilde{\varepsilon}_{l,b}(x) = \frac{1}{\Lambda} \int_0^{l\delta} \exp(-jbKx) dx \quad (\text{A7})$$

for the backward-slanted sawtooth grating, where $\delta = \Lambda/L$.

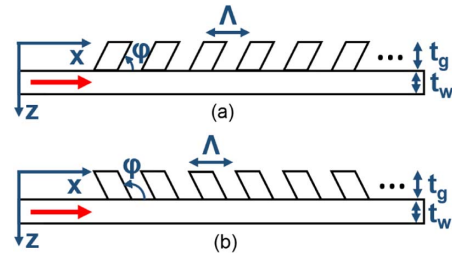


Fig. 6. Schematic representation (not to scale) of a guided wave incident on a parallelogramic grating with (a) slant angle $\varphi < 90^\circ$ or (b) $\varphi > 90^\circ$.

C. Volume Grating

Figure 9 shows the structure of a volume grating with slant angle φ . The permittivity of the volume grating varies sinusoidally, which is expressed as

$$\varepsilon_g = \varepsilon_{g0} + \Delta\varepsilon \cos(K \sin \varphi x + K \cos \varphi z), \quad (\text{A8})$$

where ε_{g0} is the average permittivity and $\Delta\varepsilon$ is the amplitude of the sinusoidal variation. The i -th propagation constant in x direction is defined as

$$k_{x,i} = k_0 n_g \sin \theta' - iK \sin \varphi, \quad (\text{A9})$$

and the i -th propagation constant in z direction in the volume grating is defined as

$$k_{z,i} = k_0 n_g \cos \theta' - iK \cos \varphi, \quad (\text{A10})$$

where $n_g = \sqrt{\varepsilon_{g0}}$ and θ' is the 0th order refraction angle inside of the grating ($k_0 n_c \sin \theta = k_0 n_g \sin \theta'$, where $k_0 = \frac{2\pi}{\lambda_0}$ and n_c

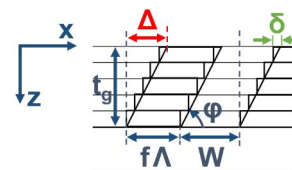


Fig. 7. Sublayers of a “forward-slanted” parallelogramic grating with $\Delta < W$.

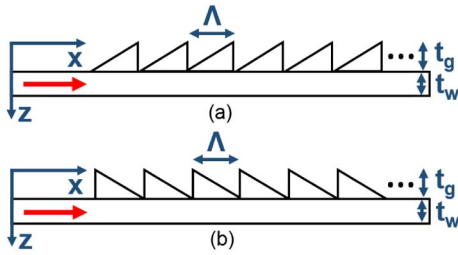


Fig. 8. Schematic representation (not to scale) of a guided wave incident on a sawtooth grating with (a) forward slanted ridges or (b) backward slanted ridges.

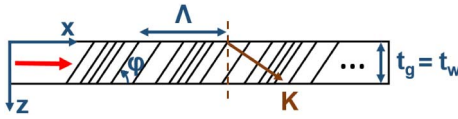


Fig. 9. Schematic representation (not to scale) of a guided wave incident on a volume grating.

is the refractive index of the cover). The electric field in the volume grating is expressed by Fourier expansions in spatial harmonics as

$$E_{gy} = \sum_i S_{gy,i} \exp(-jk_{x,i}x - jk_{gz,i}z), \quad (\text{A11})$$

and it satisfies the wave equation

$$\nabla^2 E_{gy} + k_0^2 \epsilon_g E_{gy} = 0. \quad (\text{A12})$$

Substituting Eq. (A11) into Eq. (A12) gives

$$\frac{\partial^2 S_{gy,i}}{\partial z^2} - j4\pi \left(\frac{\sqrt{\epsilon_{g0}} \cos \theta'}{\lambda} - \frac{i \cos \varphi}{\Lambda} \right) \frac{\partial S_{gy,i}}{\partial z} \quad (\text{A13})$$

$$+ \frac{4\pi^2}{\Lambda^2} i(m-i) S_{gy,i} + \frac{2\pi^2 \Delta \epsilon}{\lambda^2} (S_{gy,i+1} + S_{gy,i-1}) = 0, \quad (\text{A14})$$

where $m = \frac{2\Lambda}{\lambda} \sqrt{\epsilon_{g0}} \cos(\theta' - \varphi)$. The permittivity matrix of the volume grating can be expressed in the form of Eq. (A5) in Moharam and Gaylord [42], and the eigenvector matrix \mathbf{W} and eigenvalue matrix \mathbf{Q} of the permittivity matrix can be calculated. The electric field expression in the volume grating is expressed as

$$S_{gy,i}(z) = \sum_{p=1}^{2s} C_p w_{i,p} \exp(q_p z) \quad (\text{A15})$$

where s is the total number of diffraction orders, $w_{i,p}$ is the (i, p) th element of \mathbf{W} (size $2s \times 2s$), and q_p is the (p, p) th element of \mathbf{Q} (size $2s \times 2s$).

If the volume grating is fabricated in the waveguide, the nonhomogenous system of equations related to the boundary conditions is in the form of

$$\begin{bmatrix} -\mathbf{I} & \mathbf{0} & \mathbf{M}_{g1} \\ -j\mathbf{Y}_c & \mathbf{0} & \mathbf{M}_{g2} \\ \mathbf{0} & -\mathbf{I} & \mathbf{M}_{g3} \\ \mathbf{0} & j\mathbf{Y}_s & \mathbf{M}_{g4} \end{bmatrix} \begin{bmatrix} \mathbf{R} \\ \mathbf{T} \\ \mathbf{C}_1 \\ \mathbf{C}_2 \end{bmatrix} = \begin{bmatrix} \delta_{i0} \\ a\delta_{i0} \\ \mathbf{0} \\ \mathbf{0} \end{bmatrix}, \quad (\text{A16})$$

where $a = -jk_0 n_c \cos \theta$; \mathbf{Y}_c and \mathbf{Y}_s are diagonal matrices with diagonal elements $k_{cz,i}$ and $k_{sz,i}$ (defined in [41]), respectively; \mathbf{C}_1 and \mathbf{C}_2 are vectors consisting of C_1 to C_s and C_{s+1} to C_{2s} , respectively; \mathbf{M}_{g1} is the matrix consisting of the first s rows of \mathbf{W} ; the (i, p) th element of \mathbf{M}_{g2} is $M_{i,p}^{g1}(q_p - jk_{gz,i})$; the (i, p) th element of \mathbf{M}_{g3} is $M_{i,p}^{g1} \exp(q_p - jk_{gz,i})$; and the (i, p) th element of \mathbf{M}_{g4} is $M_{i,p}^{g1}(q_p - jk_{gz,i}) \exp(q_p - jk_{gz,i})$. The sizes of \mathbf{M}_{g1} , \mathbf{M}_{g2} , \mathbf{M}_{g3} , and \mathbf{M}_{g4} are $s \times 2s$, while the others are $s \times s$. If the volume grating is configured above the waveguide, the boundary condition matrix is in the form of Eq. (23) of [41] with appropriate modifications.

REFERENCES

1. B. Wang, J. Jiang, and G. P. Nordin, "Embedded slanted grating for vertical coupling between fibers and silicon-on-insulator planar waveguides," *IEEE Photon. Technol. Lett.* **17**, 1884–1886 (2005).
2. R. Halir, A. Ortega-Monux, J. H. Schmid, C. Alonso-Ramos, J. Lapointe, D. X. Xu, J. G. Wanguemert-Perez, I. Molina-Fernandez, and S. Janz, "Recent advances in silicon waveguide devices using sub-wavelength gratings," *IEEE J. Sel. Top. Quantum Electron.* **20**, 279–291 (2014).
3. J. Kang, Y. Atsumi, M. Oda, T. Amemiya, N. Nishiyama, and S. Arai, "Layer-to-layer grating coupler based on hydrogenated amorphous silicon for three-dimensional optical circuits," *Jpn. J. Appl. Phys.* **51**, 120203 (2012).
4. Y. Tang, D. Dai, and S. He, "Proposal for a grating waveguide serving as both a polarization splitter and an efficient coupler for silicon-on-insulator nanophotonic circuits," *IEEE Photon. Technol. Lett.* **21**, 242–244 (2009).
5. O. Solgaard, F. Sandejas, and D. Bloom, "Deformable grating optical modulator," *Opt. Lett.* **17**, 688–690 (1992).
6. Y. Shibata, S. Oku, Y. Kondo, T. Tamamura, and M. Naganuma, "Semiconductor monolithic wavelength selective router using a grating switch integrated with a directional coupler," *J. Lightwave Technol.* **14**, 1027–1032 (1996).
7. G. Li, Y. Hashimoto, T. Maruyama, and K. Iiyama, "High-efficiency optical coupling to planar photodiode using metal reflector loaded waveguide grating coupler," *Opt. Quantum Electron.* **45**, 657–663 (2013).
8. S. R. Park, O. J. Kwon, D. Shin, S.-H. Song, H.-S. Lee, and H. Y. Choi, "Grating micro-dot patterned light guide plates for LED backlights," *Opt. Express* **15**, 2888–2899 (2007).
9. K. M. Byun, S. J. Kim, and D. Kim, "Grating-coupled transmission-type surface plasmon resonance sensors based on dielectric and metallic gratings," *Appl. Opt.* **46**, 5703–5708 (2007).
10. M.-S. Kwon, "Disposable and compact integrated plasmonic sensor using a long-period grating," *Opt. Lett.* **35**, 3835–3837 (2010).
11. M. Nedeljkovic, J. S. Penades, C. J. Mitchell, A. Z. Khokhar, S. Stankovic, T. Dominguez Bucio, C. G. Littlejohns, F. Y. Gardes, and G. Z. Mashanovich, "Surface-grating-coupled low-loss Ge-on-Si rib waveguides and multimode interferometers," *IEEE Photon. Technol. Lett.* **27**, 1040–1043 (2015).
12. N. Eriksson, M. Hagberg, and A. Larsson, "Highly directional grating outcouplers with tailorable radiation characteristics," *IEEE J. Quantum Electron.* **32**, 1038–1047 (1996).
13. A. Alphones and M. Tsutsumi, "Leaky wave radiation from a periodically photexcited semiconductor slab waveguide," *IEEE Trans. Microwave Theory Tech.* **43**, 2435–2441 (1995).

14. S. H. Lin, K. Y. Hsu, W.-Z. Chen, and W. T. Whang, "Phenanthrenequinone-doped poly (methyl methacrylate) photopolymer bulk for volume holographic data storage," *Opt. Lett.* **25**, 451–453 (2000).
15. N. Plainfield, "Optical correlation technique," *Appl. Phys. Lett.* **21**, 82–83 (1962).
16. C. Gu, H. Fu, and J.-R. Lien, "Correlation patterns and cross-talk noise in volume holographic optical correlators," *J. Opt. Soc. Am. A* **12**, 861–868 (1995).
17. C.-C. Sun and W.-C. Su, "Three-dimensional shifting selectivity of random phase encoding in volume holograms," *Appl. Opt.* **40**, 1253–1260 (2001).
18. K. O. Hill and G. Meltz, "Fiber Bragg grating technology fundamentals and overview," *J. Lightwave Technol.* **15**, 1263–1276 (1997).
19. J. M. Tedesco, H. Owen, D. M. Pallister, and M. D. Morris, "Principles and spectroscopic applications of volume holographic optics," *Anal. Chem.* **65**, 441A–449A (1993).
20. H. Kogelnik, "Coupled wave theory for thick hologram gratings," *Bell Syst. Tech. J.* **48**, 2909–2947 (1969).
21. A. Tishchenko, M. Hamdoun, and O. Parriaux, "Two-dimensional coupled mode equation for grating waveguide excitation by a focused beam," *Opt. Quantum Electron.* **35**, 475–491 (2003).
22. R. S. Chu and J. A. Kong, "Modal theory of spatially periodic media," *IEEE Trans. Microwave Theory Tech.* **25**, 18–24 (1977).
23. W. Streifer, D. R. Scifres, and R. D. Burnham, "Analysis of grating-coupled radiation in GaAs: GaAlAs lasers and waveguides-I," *IEEE J. Quantum Electron.* **12**, 422–428 (1976).
24. K. Ogawa, W. S. Chang, B. L. Sopori, and F. J. Rosenbaum, "A theoretical analysis of etched grating couplers for integrated optics," *IEEE J. Quantum Electron.* **9**, 29–42 (1973).
25. A. R. Neureuther and K. Zaki, "Numerical methods for the analysis of scattering from nonplanar periodic structures," *Alta Freq.* **38**, 282–285 (1969).
26. M. Nevière, R. Petit, and M. Cadilhac, "About the theory of optical grating coupler-waveguide systems," *Opt. Commun.* **8**, 113–117 (1973).
27. S. Peng, T. Tamir, and H. L. Bertoni, "Theory of periodic dielectric waveguides," *IEEE Trans. Microwave Theory Tech.* **23**, 123–133 (1975).
28. A. Zlenko, V. Kiselev, A. Prokhorov, A. Spikhal'skii, and V. Sychugov, "Emission of surface light waves from a corrugated part of a thin-film waveguide," *Sov. J. Quantum Electron.* **4**, 839–842 (1975).
29. V. Kiselev, "Diffraction coupling of radiation into a thin-film waveguide," *Sov. J. Quantum Electron.* **4**, 872–875 (1975).
30. V. A. Sychugov, A. V. Tishchenko, B. A. Usievich, and O. Parriaux, "Optimization and control of grating coupling to or from a silicon-based optical waveguide," *Opt. Eng.* **35**, 3092–3100 (1996).
31. A. Yariv, "Coupled-mode theory for guided-wave optics," *IEEE J. Quantum Electron.* **9**, 919–933 (1973).
32. A. Spikhal'skii, V. A. Sychugov, and A. V. Tishchenko, "Simple method for calculating the optical attenuation coefficient of a corrugated waveguide," *Sov. J. Quantum Electron.* **13**, 592–595 (1983).
33. M. G. Moharam, E. B. Grann, D. A. Pommet, and T. K. Gaylord, "Formulation for stable and efficient implementation of the rigorous coupled-wave analysis of binary gratings," *J. Opt. Soc. Am. A* **12**, 1068–1076 (1995).
34. T. K. Gaylord and M. G. Moharam, "Analysis and applications of optical diffraction by gratings," *Proc. IEEE* **73**, 894–937 (1985).
35. J. Kang, Y. Atsumi, Y. Hayashi, J. Suzuki, Y. Kuno, T. Amemiya, N. Nishiyama, and S. Arai, "Amorphous-silicon inter-layer grating couplers with metal mirrors toward 3-D interconnection," *IEEE J. Sel. Top. Quantum Electron.* **4**, 1–8 (2014).
36. Y. Zhang, D. Kwong, X. Xu, A. Hosseini, S. Y. Yang, J. A. Rogers, and R. T. Chen, "On-chip intra-and inter-layer grating couplers for three-dimensional integration of silicon photonics," *Appl. Phys. Lett.* **102**, 211109 (2013).
37. M. Sodagar, R. Pourabolghasem, A. A. Eftekhari, and A. Adibi, "High-efficiency and wideband interlayer grating couplers in multilayer Si/SiO₂/SiN platform for 3D integration of optical functionalities," *Opt. Express* **22**, 16767–16777 (2014).
38. R. Shi, H. Guan, A. Novack, M. Streshinsky, A. E.-J. Lim, G.-Q. Lo, T. Baehr-Jones, and M. Hochberg, "High-efficiency grating couplers near 1310 nm fabricated by 248-nm DUV lithography," *IEEE Photon. Technol. Lett.* **26**, 1569–1572 (2014).
39. R. A. Villalaz, E. N. Glytsis, and T. K. Gaylord, "Volume grating couplers: polarization and loss effects," *Appl. Opt.* **41**, 5223–5229 (2002).
40. S. M. Schultz, E. N. Glytsis, and T. K. Gaylord, "Design of a high-efficiency volume grating coupler for line focusing," *Appl. Opt.* **37**, 2278–2287 (1998).
41. C. Wan, T. K. Gaylord, and M. S. Bakir, "Grating design for interlayer optical interconnection of in-plane waveguides," *Appl. Opt.* **55**, 2601–2610 (2016).
42. M. G. Moharam and T. K. Gaylord, "Rigorous coupled-wave analysis of planar-grating diffraction," *J. Opt. Soc. Am.* **71**, 811–818 (1981).
43. E. Anemogiannis and E. N. Glytsis, "Multilayer waveguides: efficient numerical analysis of general structures," *J. Lightwave Technol.* **10**, 1344–1351 (1992).
44. M. Li and S. J. Sheard, "Waveguide couplers using parallelogram-shaped blazed gratings," *Opt. Commun.* **109**, 239–245 (1994).
45. D. Marcuse, "Exact theory of TE-wave scattering from blazed dielectric gratings," *Bell Syst. Tech. J.* **55**, 1295–1317 (1976).
46. W. Streifer, R. D. Burnham, and D. R. Scifres, "Analysis of grating-coupled radiation in GaAs: GaAlAs lasers and waveguides-II: blazing effects," *IEEE J. Quantum Electron.* **12**, 494–499 (1976).
47. K. C. Chang and T. Tamir, "Simplified approach to surface-wave scattering by blazed dielectric gratings," *Appl. Opt.* **19**, 282–288 (1980).
48. S. Peng and T. Tamir, "Directional blazing of waves guided by asymmetrical dielectric gratings," *Opt. Commun.* **11**, 405–409 (1974).
49. M. Li and S. J. Sheard, "Experimental study of waveguide grating couplers with parallelogramic tooth profiles," *Opt. Eng.* **35**, 3101–3106 (1996).
50. T. Liao, S. Sheard, M. Li, J. Zhu, and P. Prewett, "High-efficiency focusing waveguide grating coupler with parallelogramic groove profiles," *J. Lightwave Technol.* **15**, 1142–1148 (1997).
51. T. Aoyagi, Y. Aoyagi, and S. Namba, "High-efficiency blazed grating couplers," *Appl. Phys. Lett.* **29**, 303–304 (1976).